

This is an Open Access document downloaded from ORCA, Cardiff University's institutional repository: <https://orca.cardiff.ac.uk/id/eprint/117571/>

This is the author's version of a work that was submitted to / accepted for publication.

Citation for final published version:

Perepelkin, Nikolay , Kovalev, Alexander E., Gorb, Stanislav N. and Borodich, Feodor M. 2019. Estimation of the elastic modulus and the work of adhesion of soft materials using the extended Borodich-Galanov (BG) method and depth sensing indentation. *Mechanics of Materials* 129 , pp. 198-213.
10.1016/j.mechmat.2018.11.017

Publishers page: <http://dx.doi.org/10.1016/j.mechmat.2018.11.017>

Please note:

Changes made as a result of publishing processes such as copy-editing, formatting and page numbers may not be reflected in this version. For the definitive version of this publication, please refer to the published source. You are advised to consult the publisher's version if you wish to cite this paper.

This version is being made available in accordance with publisher policies. See <http://orca.cf.ac.uk/policies.html> for usage policies. Copyright and moral rights for publications made available in ORCA are retained by the copyright holders.



Estimation of the elastic modulus and the work of adhesion of soft materials using the extended Borodich-Galanov (BG) method and depth sensing indentation

Nikolay V. Perepelkin^{a,c,*}, Alexander E. Kovalev^b, Stanislav N. Gorb^b,
Feodor M. Borodich^a

^a*School of Engineering, Cardiff University, Cardiff, CF24 3AA, UK*

^b*Department of Functional Morphology and Biomechanics, Zoological Institute of the University of Kiel, Am Botanischen Garten 1-9, D-24098, Kiel, Germany*

^c*Department of Applied Mathematics, National Technical University "Kharkiv Polytechnic Institute", 2 Kyrpychova Str, Kharkiv, 61002, Ukraine*

Abstract

The depth-sensing indentation (DSI) is currently one of the main experimental techniques for studying elastic properties of materials of small volumes. Usually DSI tests are performed using sharp pyramidal indenters and the load-displacement curves obtained are used for estimations of elastic moduli of materials, while the curve analysis for these estimations is based on the assumptions of the Hertz contact theory of non-adhesive contact. The Borodich-Galanov (BG) method provides an alternative methodology for estimations of the elastic moduli along with estimations of the work of adhesion of the contacting pair in a single experiment using the experimental DSI data for spherical indenters. The method assumes fitting the experimental points of the load-displacement curves using a dimensionless expression of an appropriate theory of adhesive contact. Earlier numerical simulations showed that the BG method was robust. Here first the original BG method is modified and then its accuracy in the estimation of the reduced elastic modulus is directly tested by comparison with the results of conventional tensile tests.

The method modification is twofold: (i) a two-stage fitting of the theoret-

*Corresponding author

Email address: PerepelkinM@cardiff.ac.uk (Nikolay V. Perepelkin)

ical DSI dependency to the experimental data is used and (ii) a new objective functional is introduced which minimizes the squared norm of difference between the theoretical curve and the one used in preliminary data fitting. The direct experimental validation of accuracy and robustness of the BG method has two independent steps. First the material properties of polyvinyl siloxane (PVS) are determined from a DSI data by means of the modified BG method; and then the obtained results for the reduced elastic modulus are compared with the results of tensile tests on dumbbell specimens made of the same charge of PVS.

Comparison of the results of the two experiments showed that the absolute minimum in relative difference between individual identified values of the reduced elastic modulus in the two experiments was 3.80%; the absolute maximum of the same quantity was 27.38%; the relative difference in averaged values of the reduced elastic modulus varied in the range 16.20 ... 17.09% depending on particular settings used during preliminary fitting. Hence, the comparison of the results shows that the experimental values of the elastic modulus obtained by the tensile tests are in good agreement with the results of the extended BG method. Our analysis shows that unaccounted factors and phenomena tend to decrease the difference in the results of the two experiments. Thus, the robustness and accuracy of the proposed extension of the BG method has been directly validated.

Keywords: the BG method, estimation of material properties, depth sensing indentation, tensile testing, polyvinyl siloxane (PVS)

1. Introduction

Evaluation of elastic moduli of materials and their adhesive properties is one of the important tasks of modern materials science. However, the experimental estimations of the material properties become particularly challenging if the specimen is made of a small quantity of material or if it is a thin film deposited on the surface of another object. In these cases one of the most useful techniques is the depth sensing indentation (DSI). This technique includes loading and unloading of a material specimen by a probe (indenter), and continuous monitoring the value of the applied force (P) and the probe displacement (δ).

DSI was introduced by Kalei (1968) 50 years ago. Then it was suggested to use the experimental unloading $P - \delta$ curves for extracting the values

of the elastic modulus of the tested material (Bulychev et al., 1975, 1976; Shorshorov et al., 1981). Currently there are several approaches for evaluation of the elastic modulus employing the DSI experiments with sharp pyramidal indenters (Doerner and Nix, 1986; Oliver and Pharr, 1992; Bull, 2005; Galanov and Dub, 2017). On the other hand, the DSI technique works with spherical indenters too. One of the techniques based on an inverse analysis of the DSI experiments with spherical indenters is the BG method. Originally the BG method was introduced by Borodich and Galanov (2008) and then it was discussed in a series of papers (Borodich et al., 2012a,b, 2013). Numerical tests and experimental studies showed that even the original BG method is simple and robust. Our paper is devoted to the extension of the BG method and direct experimental validation of both the accuracy and robustness of this extended method.

To explain the advantages of the BG approach, we need to discuss the common DSI techniques working with pyramidal indenters first. In the above cited approaches to DSI by sharp indenters, the unknown elastic properties of samples are estimated from the experimental DSI data by solving an inverse problem to the non-adhesive Hertz-type contact problem (see e.g., Johnson (1985); Popov (2010); Borodich (2014)). As any other model-based approaches, it requires a prebuilt mathematical model of the interaction between the probe and the specimen. It follows from the Hertz contact theory that the elastic modulus may be estimated using the BASH (Bulychev–Alekhin–Shorshorov) formula. Originally formula was derived for frictionless contact of some axisymmetric punches and it was suggested to extend it to non-axisymmetric indenters, e.g. pyramidal indenters (Bulychev et al., 1975). Then it was noted that if one applies the geometrically linear formulation of Hertz-type contact problem to unloading branch of the $P - \delta$ curve then one needs to take into account the actual distance between the indenter and the plastically distorted surface (the Galanov effect) (Galanov et al., 1983, 1984). It was also shown that the friction between the indenter and the specimen surface may also affect the slope of the unloading curve (Borodich and Keer, 2004b). Thus, the BASH formula can be written as (Argatov et al., 2017)

$$\frac{dP}{d\delta} = \beta \frac{2}{\sqrt{\pi}} E^* \sqrt{A}, \quad \beta = \beta_1 \cdot \beta_2 \cdot \beta_3 \quad (1)$$

where A is the area of the contact region and E^* is the reduced elastic contact modulus. For isotropic materials, this modulus can be obtained from the

following formula

$$\frac{1}{E^*} = \frac{1 - \nu_1^2}{E_1} + \frac{1 - \nu_2^2}{E_2}$$

where E_i and ν_i ($i = 1, 2$) are the elastic modulus and Poisson's ratio of the two contacting solids (the specimen and the indenter) respectively. If the indenter is rigid, i.e. $E_2 = \infty$ then $E^* = E/(1 - \nu^2)$ where $E = E_1$ and $\nu = \nu_1$ are the elastic modulus and Poisson's ratio of the half-space, respectively. In (1) the factor β_1 is introduced due to the concept of the effective indenter shape (the Galanov effect) (Galanov et al., 1983, 1984), β_2 is the contact area shape factor which extends the BASH formula to the non-axisymmetric case, and the factor β_3 is introduced due to the effects of friction between the indenter and the half-space (Borodich and Keer, 2004a,b). It has been shown in the case of adhesive (no-slip) contact between a rigid indenter and an elastic sample $\beta_3 = C_{NS}$ that can be expressed as a function of the material Poisson ratio (ν)

$$C_{NS} = \frac{(1 - \nu) \ln(3 - 4\nu)}{1 - 2\nu}. \quad (2)$$

The above described approaches to indentation by sharp indenters have several drawbacks. Strictly speaking the Hertz contact theory is not applicable to these tests based on the use of sharp indenters (see a discussion in Borodich and Keer (2004a); Chaudhri and Lim (2007); Borodich (2014)), in addition, it ignores the adhesive effects between the indenter and the sample. On the other hand, the use of spherical indenters allows the researchers to avoid plastic deformations of specimens and therefore, they may work in the framework of theory of elasticity and do not violate the geometrical assumptions of the Hertz formulation. In addition, devices with cantilever-supported indenters may be used. In the case of cantilever support the inavoidable inclination of the cantilever (see e.g. Al-Musawi et al. (2016)) has much less influence on interaction between the indenter and the specimen in comparison to the case when a sharp indenter is used.

The original version of the BG method is based on solving an inverse problem to adhesive contact between a spherical indenter and an elastic half-space using one of the well-established theories of adhesive contact, e.g. the JKR or DMT ones. The method uses a dimensionless mathematical dependency between the force applied to the indenter and its displacement (the theoretical load-displacement curve) as the mathematical model of the adhesive interaction "indenter-specimen".

Any analytical force-displacement dependency can be written in a dimensionless form. To do so, one needs to determine the so-called characteristic scales of the problem. These scales are the model parameters and their values are subject to adjustment through an optimization process until the best fit of the theoretical curve to the experimental data points is found. The particular representation of the theoretical curve and the characteristic scales depends on the theory of adhesive contact chosen as the framework of the problem (e.g. the Johnson-Kendall-Roberts (JKR)(Johnson et al., 1971) or the Derjaguin-Muller-Toporov (DMT)(Derjaguin et al., 1975) theories). For example, for a spherical indenter of radius R , the characteristic scales may be taken as

$$P_c = \frac{3}{2}\pi w R, \quad \delta_c = \frac{3}{4} \left(\frac{\pi^2 w^2 R}{E^{*2}} \right)^{1/3}. \quad (3)$$

In the JKR theory, the above characteristic scales have a clear mechanical meaning: P_c is denoted the absolute value of the pull-off force, and δ_c is the absolute value of the minimum displacement that occurs due to adhesion. Once optimal values of P_c and δ_c are found, the material properties E^* and w can be easily evaluated by inversion of the latter formulae

$$w = \frac{2P_c}{3\pi R}, \quad E^* = \frac{P_c}{4} \sqrt{\frac{3}{R\delta_c^3}}. \quad (4)$$

Contrary to the interpretation of the DSI tests based on the BASH formula, the BG method allows not only to evaluate the elastic properties (the reduced elastic contact modulus E^*) but also the adhesive properties (the work of adhesion w) of tested pair of materials. Unlike the other methods of mechanics of materials that require separate experimental set-ups for the determination of elastic and adhesive properties of materials, the BG method allows to identify those quantities simultaneously using a single set-up. Moreover, it can utilize only the stable compressive part of the load-displacement data whereas some other approaches require the pull-off force measurements in order to estimate the value of the work of adhesion (e.g. Ebenstein and Wahl (2006); Carrillo et al. (2005); Rundlöf et al. (2000); Wahl et al. (2006); Yu et al. (2015)). However, measurements of the pull-off force can be influenced by many factors: the roughness of contacting surfaces, surface chemistry, wear of the DSI probe, chemical modification of its surface (in case of atomic force microscopy used), dust particles etc. (see e.g., Grierson et al.

(2005); Beach et al. (2002); Gorb and Gorb (2009)). Therefore, the tensile part of DSI load-displacement data can be considered unstable and less trustworthy, and the BG method has an advantage here.

The BG method is non-direct because the characteristic values are not measured but rather evaluated from the stable part of the $P - \delta$ diagram, while P_c is extracted from measurements on the unstable part of the diagram in the direct methods (Wahl et al., 2006; Ebenstein and Wahl, 2006). In addition, the BG method differs from the ordinary least-squares fitting because: (i) it uses different objective functional and therefore, it provides different optimum, (ii) whenever possible, dimensionless variables are used which allows to apply optimization procedures to the quantities of different physical nature and different orders of magnitude.

The paper is organized as follows. In Section 2, the paradigm of the BG method is extended. Originally the method was applied only to the contact problem between a spherical indenter and an elastic half-space. Here, it is argued that the BG method can be considered as a general model-based approach to determination of the effective contact modulus and the work of adhesion of materials or structures from the DSI data. Examples of appropriate theories of adhesive contact and the corresponding theoretical load-displacement curves are considered. Then an alternative formulation of the objective functional of the BG method is also given. A concept of two-stage fitting of the theoretical DSI dependency to the experimental data points is introduced. This means that the data is fitted firstly by an auxiliary curve which acts as a filter in certain sense. The mathematical representation of that pre-fitting curve is supposed to be as simple as possible. This allows one to use some advanced fitting/filtering techniques to reduce measurement noise and fluctuations in the data. Secondly, the theoretical load-displacement curve (the expected DSI dependency which may be a complex expression) is fitted to the auxiliary one via minimization of the squared norm of the difference of the two functions (the objective functional). The sought material properties are determined from the optimal set of characteristic parameters that give minimum to the objective functional.

In Section 3 the results of a DSI-based experiment and an application of the extended BG method are described. The experimental set-up and raw data pre-processing are also discussed. A specimen was made of polyvinyl siloxane (PVS). This is an elastomer widely used as an impression material, particularly in dentistry. A series of DSI tests was carried out using DSI equipment and a spherical indenter (lens) of large radius ($R = 5.155$ mm)

supported by a cantilever spring with constant $c = 1023.9\text{N/m}$. The experimental data was processed using the extended BG method, and the values of the modulus E^* and the work of adhesion w were calculated. The specimen size was large enough to consider it as an elastic half-space, and therefore, the JKR theory of adhesive contact was applied.

In Section 4 the description of the tensile set-up used for the validation of the BG method is given as well as the discussion regarding post-processing of the measured data and the obtained results. In this experiment we performed conventional tensile testing (Davis, 2004) of ISO 37 type 3 dumbbell specimens made of exactly the same PVS material using Zwick Roell tensile machine. As the result of this experiment, the elastic modulus E and Poisson's ratio ν were determined which allowed us to calculate the reduced elastic contact modulus $E^* = E/(1 - \nu^2)$ and compare it to the value obtained using the BG method. Since our piece of equipment was not equipped with extensometer, two types of mathematical modelling (analytical and finite element) of the tensile experiment was used to introduce correction into the values of E produced from the raw tensile data. The value of Poisson's ratio was estimated from video records of stretching process by using the methods of photogrammetry.

In Section 5, the results of the two experiments are compared and the used approaches discussed. It is shown that the values of E^* calculated using the two different approaches coincide well. Our analysis shows that unaccounted factors and phenomena tend to decrease the difference in the results of the two experiments. Thus, the accuracy of the BG method has been directly validated in this work. The obtained results also provide more experimental data on PVS properties, since this matter is not widely represented in literature (see e.g., Chai et al. (1998); Wieckiewicz et al. (2016))

2. The extended BG method

As it is mentioned above, the BG method allows one to extract from the experimental data of DSI test the two properties of the tested material simultaneously: the reduced elastic contact modulus E^* and the work of adhesion w . The BG method in its original form presumes the use of either the JKR or the DMT theories of adhesive contact between a spherical indenter and an elastic half-space. The load-displacement relation in these theories can be

represented in the dimensionless form as

$$F\left(\frac{P}{P_c}, \frac{\delta}{\delta_c}\right) = 0. \quad (5)$$

Let us consider a set of N measured experimental values of indentation depth δ_i and indentation force P_i : (δ_i, P_i) , $i = 1, \dots, N$. If the measurements are absolutely exact, then the values of P_c and δ_c can be determined quite easily. Indeed, the theoretical curve in such case passes through all the data points which can be mathematically expressed as the set of equalities

$$F\left(\frac{P_i}{P_c}, \frac{\delta_i}{\delta_c}\right) = 0, \quad i = 1, \dots, N. \quad (6)$$

The correct values of P_c and δ_c make all of these equations valid simultaneously. Therefore, one needs to take any two of them and solve for P_c and δ_c . However, the real experimental measurements (δ_i, P_i) always contain some measurement errors. Therefore, one needs to take into account all of the N expressions in (6) simultaneously. Due to measurement errors the expressions (6) never become true at the same time and the inverse problem of finding the characteristic scales from the DSI data is ill-defined (one has an overdetermined system of equations) (Borodich and Galanov, 2008).

Since it is impossible to make all of the expressions in (6) true, one can only minimize the measure of the overall 'error' produced in (6). If $\varepsilon_i = F\left(\frac{P_i}{P_c}, \frac{\delta_i}{\delta_c}\right)$ is the residual of i -th equation, then the measure of the total 'error' can be the mean square value of all such residuals

$$\epsilon = \frac{1}{N} \sum_{i=1}^N \varepsilon_i^2. \quad (7)$$

Hence, in order to find the appropriate values of the characteristic parameters an optimization problem must be solved. The optimal values of the characteristic parameters P_c^*, δ_c^* that minimize the mean square residual (7) of the equations (6) are found as the result of minimization of the objective functional (the cost functional) of the problem $\Phi(P_c, \delta_c)$

$$\{P_c^*, \delta_c^*\} = \arg \min \Phi(P_c, \delta_c) \quad (8)$$

where

$$\Phi(P_c, \delta_c) = \sum_{i=1}^N \left[F \left(\frac{P_i}{P_c}, \frac{\delta_i}{\delta_c} \right) \right]^2. \quad (9)$$

After the above optimization problem is solved (see e.g., Boyd and Vandenberghe (2004); Chong and Zak (2001)), the theoretical curve (5) becomes best fit to the experimental data in the sense of (9) through the choice $P_c = P_c^*$ and $\delta_c = \delta_c^*$ and the sought material parameters E^* and w can be evaluated using (4).

In particular, if the JKR theory of adhesive contact (Johnson et al., 1971) is used, then the load-displacement dependency can be written as a piece-wise function of the form

$$\begin{cases} (3\chi - 1) \left(\frac{1 + \chi}{9} \right)^{\frac{1}{3}} - \frac{\delta}{\delta_c} = 0 \\ \text{for } \chi \geq 0, \frac{\delta}{\delta_c} \geq -3^{-2/3}, \\ \\ (3\chi + 1) \left(\frac{1 - \chi}{9} \right)^{\frac{1}{3}} - \frac{\delta}{\delta_c} = 0 \\ \text{for } \frac{2}{3} \geq \chi \geq 0, -3^{-2/3} > \frac{\delta}{\delta_c} \geq -1 \end{cases} \quad (10)$$

where $\chi = \sqrt{1 + \frac{P}{P_c}}$ (Maugis, 2000). As mentioned earlier, the characteristic scales P_c and δ_c are expressed as (3) for spherical indenter.

The experimental data is fitted with the stable part of the above dependency which becomes the function $F \left(\frac{P}{P_c}, \frac{\delta}{\delta_c} \right)$ in the BG method:

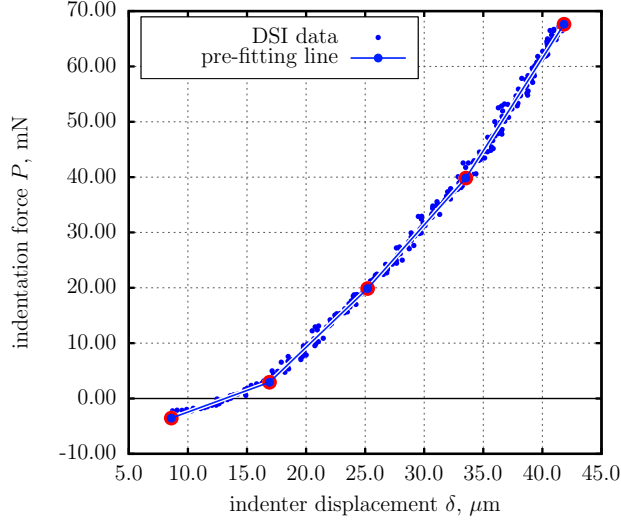
$$F \left(\frac{P}{P_c}, \frac{\delta}{\delta_c} \right) = (3\chi - 1) \left(\frac{1 + \chi}{9} \right)^{\frac{1}{3}} - \frac{\delta}{\delta_c} = 0. \quad (11)$$

As compared to the fitting approaches used by other researchers, the BG method (8)-(9) has its own distinctive features: (i) the metric (9) differs from the one normally introduced in least-squares curve fitting, therefore producing different optimum point, (ii) the method uses fitting curve written in dimensionless form which allows to treat quantities of different orders of magnitude in the same way, (iii) the fitting process is performed via adjusting characteristic scales P_c and δ_c and not the material properties. Also

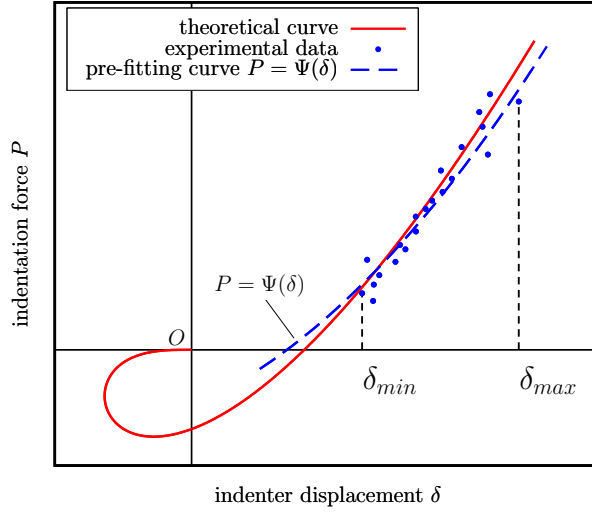
the method successfully allows to estimate E^* and w using only *compressive* part of the load-displacement data, thus using only *stable measurements* (Borodich et al., 2012a,b).

In the present paper, however, we use a variant of the extended BG method. This approach is particularly useful for the cases when the theoretical load-displacement curve is represented as a parametric function.

In this approach we first fit the experimental data with an auxiliary curve $P = \Psi(\delta)$ with low number of degrees of freedom. The curve acts as a high-pass filter, smoothing the data significantly (see Fig. 1,a). In the current work this smoothing curve was chosen to be a polygonal chain with relatively small number of segments N_S .



(a)



(b)

Figure 1: The concept of two-stage fitting the experimental data: (a) smoothing experimental data using a polygonal chain (the preliminary fitting with an auxiliary curve), (b) fitting the theoretical load-displacement curve to the auxiliary one.

The point of doing so is that the auxiliary curve is supposed to have very simple mathematical representation. Therefore, some advanced fitting methods can be used to construct it. In this work the smoothing dimensionless curve is built as the result of minimization of the sum of squares of orthogonal

distances from it to the data points (the so-called orthogonal distance fitting concept, ODF (Ahn, 2004; Boggs et al., 1987)). This approach is useful when both abscissas and ordinates of the data points are subject to measurement errors. Since the distance from a point to a straight line can be presented as a well-known formula, it is possible to *explicitly* program a function evaluating the sum of squared orthogonal distances and made it the subject of minimization process. Due to simple mathematical form (piece-wise linear), fitting with polygonal chain is performed extremely quickly using well-known computer algebra systems (e.g. Matlab).

It is important to note that the term "distance" cannot be directly applied to the space of variables of different physical meaning and of different orders of magnitude. That is the reason why the preliminary orthogonal distance fitting is performed using the normalized data:

$$\begin{aligned}\overline{\delta}_n &= \frac{\delta_n - \langle \delta_i \rangle}{\max(\delta_i) - \min(\delta_i)}, \\ \overline{P}_n &= \frac{P_n - \langle P_i \rangle}{\max(P_i) - \min(P_i)}, \\ i, n &= 1, \dots, N.\end{aligned}\tag{12}$$

where $\langle \cdot \rangle$ is the following averaging operator

$$\langle x_i \rangle = \frac{1}{N} \sum_{i=1}^N x_i.$$

This kind of normalization transforms all dimensionless values of force \overline{P}_n and displacement $\overline{\delta}_n$ into the interval $[-1, 1]$. When the coordinates of optimal polygonal chain are found in the space of the dimensionless quantities, they can be easily recalculated back to the space of dimensional quantities by inverting the formulae (12).

The particular way of construction of the pre-fitting polygonal chain was chosen as follows. The polygonal chain is supposed to have N_S segments and $N_S + 1$ vertices. The first vertex is located at δ_{min} , the last one is located at δ_{max} (see Fig. 1,b for reference). The abscissas of the vertices are uniformly spaced: the k -th vertex abscissa is $\delta_{V_k} = \delta_{min} + (\delta_{max} - \delta_{min})(k - 1)/N_S$. The ordinates of the vertices P_{V_k} are subject to optimal fitting the polygonal

chain to the data by means of the ODF fitting in the space of dimensionless quantities (12).

On the second step of the extended BG method the theoretical curve (10) is fitted to the auxiliary one via adjusting P_c and δ_c . We require minimization of the squared norm of the difference between the two functions on the interval $[\delta_{min}, \delta_{max}]$ where $\delta_{min} = \min(\delta_i)$, $\delta_{max} = \max(\delta_i)$, $i = 1, \dots, N$ (Fig. 1,b):

$$\Phi(P_c, \delta_c) = \int_{\delta_{min}}^{\delta_{max}} [P(\delta) - \Psi(\delta)]^2 d\delta \rightarrow \min. \quad (13)$$

Here $P = P(\delta)$ is the theoretical load-displacement curve, and $P = \Psi(\delta)$ is the auxiliary one.

Since the stable branch of (10) cannot be written as $P = P(\delta)$, we transform (13) as follows. Firstly, a dimensionless parameter \bar{a} along the theoretical curve is introduced as $P = P_c \bar{a}$. Secondly, the stable branch of the theoretical JKR curve (10) is rewritten in parametric form as

$$\begin{cases} \delta = \delta_c \left(3\sqrt{1 + \bar{a}} - 1 \right) \left(\frac{1 + \sqrt{1 + \bar{a}}}{9} \right)^{\frac{1}{3}}, \\ P = P_c \bar{a} \end{cases}, \quad (14)$$

or

$$\begin{cases} \delta = \delta_c f(\bar{a}), \\ P = P_c \bar{a}. \end{cases} \quad (15)$$

Substitution of (15) into (13) yields:

$$\Phi(P_c, \delta_c) = \delta_c \int_{\bar{a}_{min}}^{\bar{a}_{max}} [P_c \bar{a} - \Psi(\delta_c f(\bar{a}))]^2 \frac{df}{d\bar{a}} d\bar{a} \rightarrow \min. \quad (16)$$

The problem (16) is the particular one used in the present study to calculate the optimal values of P_c and δ_c . It was done for every separate measurement (data set) and the corresponding values of E^* and w were calculated using (3).

In the general case of parametrically-represented load-displacement curve

$$\begin{cases} \delta = \delta_c f_1(\bar{a}, \delta_c, P_c), \\ P = P_c f_2(\bar{a}, \delta_c, P_c), \end{cases} \quad (17)$$

the optimization problem (16) becomes

$$\Phi(P_c, \delta_c) = \delta_c \int_{\bar{a}_{min}}^{\bar{a}_{max}} [P_c f_2(\dots) - \Psi(\delta_c f_1(\dots))]^2 \frac{\partial f_1(\dots)}{\partial \bar{a}} d\bar{a} \rightarrow \min \quad (18)$$

where (...) denotes (\bar{a}, δ_c, P_c) .

Remark. The actual distance from the probe surface to the specimen surface is unknown. The moment when the indenter jumps into contact due to adhesion forces during loading is rather unclear due to measurement noise. This means that the origin of the δ axis is in fact unknown. Therefore, in the light of the above the measured values of δ are supposed to have an unknown additional shift value δ_s (separate for each of the DSI data sets) introduced into the readings. This value is determined as follows. A series of possible shift values is generated. Each such value is subtracted from the measured set δ_i ($i = 1, \dots, N$) and then minimization of (16) is performed. The correct shift value is supposed to give the absolute minimum of the functional values among all trial minimizations. The corresponding values of P_c and δ_c are considered to be the true ones.

3. Determination of material propertieess from a DSI experiment by the extended BG method

Let us describe a DSI-based experiment that was carried out in order to test the robustness of the modified BG method using real experimental data.

3.1. The experimental set-up and raw data pre-processing. Assumptions validation

The custom made force measurement device Basalt-1 (TETRA GmbH, Ilmenau, Germany) was used for DSI experiments (Fig. 2). In this set-up, the PVS specimen was loaded by a spherical indenter (a glass lens of known radius $R = 5.155$ mm) attached at the end of a planar cantilever spring with constant $c = 1023.9$ N/m. The displacement of the other end of the spring

was set using a piezo drive. Two fiber optical sensors S₁ and S₂ were used to control the deflections of both ends of the spring. The readings from the sensor S₂ went to the output file as total displacement δ_0 while the difference in the readings of S₁ and S₂ was recalculated into the values of applied force (in device-dependent arbitrary units) which also went to the output file. The latter values were converted to Newtons using the results of calibration.

To obtain the load-displacement dependency of the indenter, one needs to subtract the deformation of the spring from the total recorded displacement applied to the system "spring-indenter-specimen". It was done using the following formula

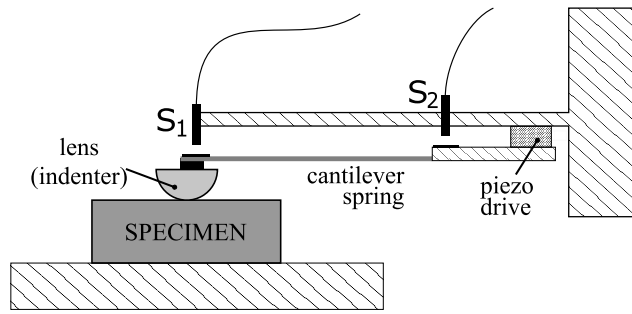
$$\delta = \delta_0 - \frac{P}{c} \quad (19)$$

where δ_0 is the total displacement applied via piezoelement, δ is the displacement of the indenter (the true displacement), P is the applied force, c is the spring stiffness.

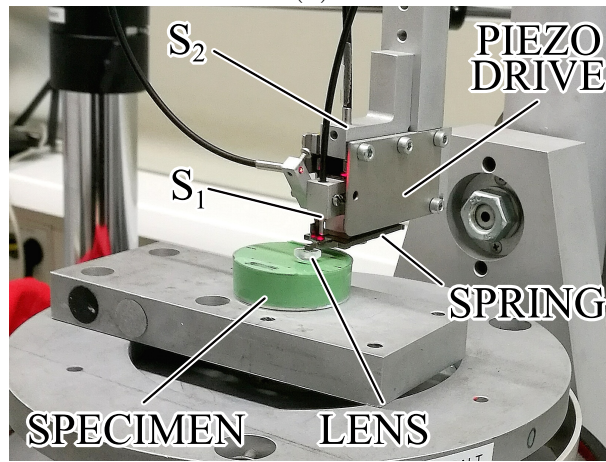
Since some measurements exhibited drift of zero point in the force value, the values of force were manually corrected for each measurement by means of a custom Matlab script. The same script was used to subtract the deformation of the spring which was done using the modified formula (19):

$$\delta = \delta_0 - \frac{P - P_{corr}}{c}$$

where P_{corr} is zero drift value. The typical processed readings are represented in Fig. 3.



(a)



(b)

Figure 2: The DSI setup: (a) the schematic, (b) the photographic image.

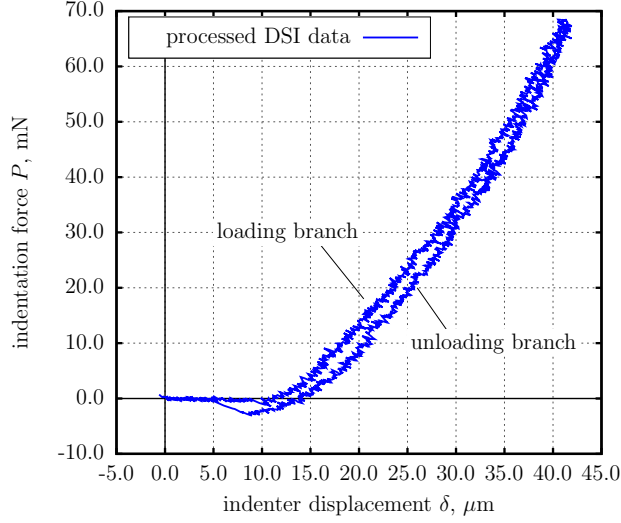


Figure 3: Typical processed DSI data (spring deflection subtracted, force readings rescaled to Newtons)

The specimen for DSI study consisted of a 35(diameter) x 10(height) mm Petri dish filled with two-component AFFINIS (R) light body PVS (Coltene, Switzerland) (Fig. 4,a). After filling the dish the PVS surface was covered with a clean piece of glass slide (Carl Roth, Karlsruhe, Germany) until the PVS polymerized in order to produce flat clean surface. Since PVS tends to form bubbles during moulding process, the top surface of the specimen was visually examined using optical microscope and 5 indentation locations were selected far from any visible inhomogeneity. Schematically the specimen is represented in Fig. 4,b, numbers denote measurement locations. Five DSI measurement were performed at each location which resulted in 25 data sets in total. Maximum indentation depth did not exceed 40 μm in each single experiment. The specimen was tested after approximately 16 h after polymerization.

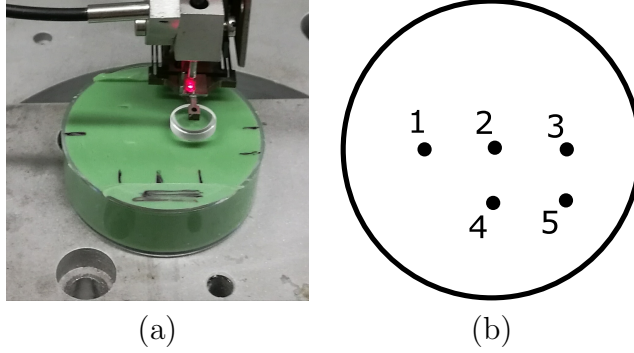


Figure 4: The PVS specimen for DSI experiment: (a) the photographic image, (b) the schematic image. Numbers denote locations of individual DSI experiments.

In the present work we model interaction between the indenter and the specimen as indentation of an elastic half-space. Indeed, many authors modelled indentation of finite-size specimens by means of the finite element method (FEM) (see e.g. Sadeghipour et al. (1994)). These studies show that a large enough finite specimen acts effectively as an elastic half-space. To confirm this for the particular geometry of our specimen we use FEM in application to the problem of non-adhesive indentation of the finite volume cylindrical specimen of radius r and height h by a rigid sphere (see the model in Fig. 5,a) The modeling was performed by means of ANSYS 18 Mechanical APDL software (<https://www.ansys.com/products/structures/ansys-mechanical-pro>) in axisymmetric formulation using the following finite element types: PLANE183 for PVS; CONTA175 and TARGE169 for contact pair (the description of these element types can be found in the ANSYS software manual or in the SNARCNET academic network https://www.sharcnet.ca/Software/Ansys/17.2/en-us/help/ans_elem/Hlp_E_ElemTOC.html). The indenter was assumed to be rigid, the PVS bulk was assumed to have the following properties: $E = 2.97$ MPa, $\nu = 0.418$. Indentation depth was supposed to be $\delta = 40\mu\text{m}$. The obtained numerically load-displacement curves for different sizes of the specimen are shown in Fig. 5,b. The reference curve obtained from Hertz contact theory for a rigid sphere and an elastic half-space is shown as well (thick solid line).

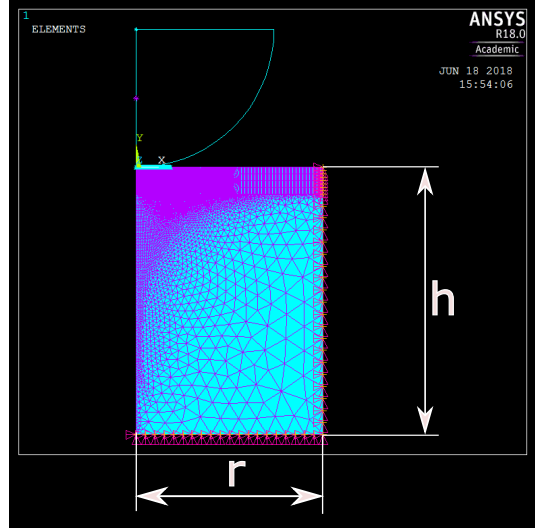
In these results the dashed line corresponds to measurement point No.2 on the specimen ($r=17$ mm, $h=10$ mm), while the thin solid line represents the case which is *worse* than any of the points No. 1,3,4 and 5 ($r=7$ mm, $h=10$ mm). Comparison the latter two simulations at the maximum indentation

depth and the Hertzian model give the relative error in force value of 4.6% and 6.6% correspondingly. Since FEM also introduces some inaccuracy in comparison to the analytical Hertzian curve, the above results are compared with the results of FEM simulation of a very large specimen ($r=68$ mm, $h=40$ mm, dots in Fig. 5) which gives the relative error of 3.9% and 5.8%, correspondingly.

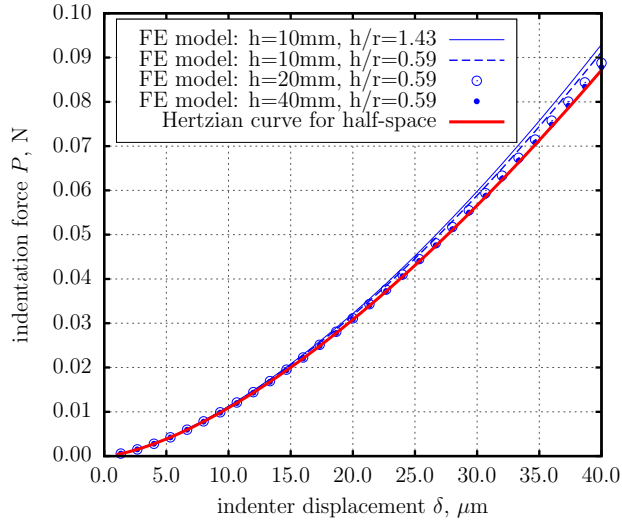
Thus, modeling the actual specimen as an infinite elastic half-space provides acceptable level of accuracy. Therefore, the mathematical apparatus of the JKR theory of adhesive contact can be applied here.

Based on the above justification, the BG method was applied to the unloading parts of the $P-\delta$ curves using the classic JKR contact theory as the framework for the problem. The theoretical load-displacement dependency was supposed to have the form (10) and the BG method was used in the extended formulation (16).

The results of application of the BG method to the obtained experimental data are described below.



(a)



(b)

Figure 5: Numerical modelling of indentation of a finite size specimen : (a) FEM model (axisymmetric, the right part of the axial cross-section is shown), (b) comparison of load-displacement curves obtained for different r and h : thick solid line (red) is the reference Hertzian curve for half-space; thin solid line (blue) corresponds to $h=10$ mm ($h/r = 1.43$); dashed line to $h=10$ mm ($h/r = 0.59$); circles to $h=20$ mm ($h/r = 0.59$); and dots to $h=40$ mm ($h/r = 0.59$).

3.2. The results of the DSI experiment

As it is mentioned above, 25 data sets representing unloading branches of the DSI curves were obtained in the experiment. Each of these data sets was pre-fitted with a polygonal chain. These lines were used as the pre-fitting function $P = \Psi(\delta)$ in (16). Since the number of segments in the pre-fitting polygonal chain has some influence on the identified values of E^* and w , the number of segments was varied from 4 to 10. Every time the values of E^* and w were identified separately for each of the 25 data sets. Then the averaged values $\langle E^* \rangle$ and $\langle w \rangle$ as well as the standard deviations σ_{E^*} and σ_w were computed.

As an example, in Fig. 6 the results of identification are shown for pre-fitting with 7-segment line. The complete result set is shown in the Appendix in Fig. A.19-A.21. It can be seen that the points on the (w, E^*) plane obtained using the modified BG method build very compact groups which shows that the approach (16) is robust against the measurement noise and fluctuations in data.

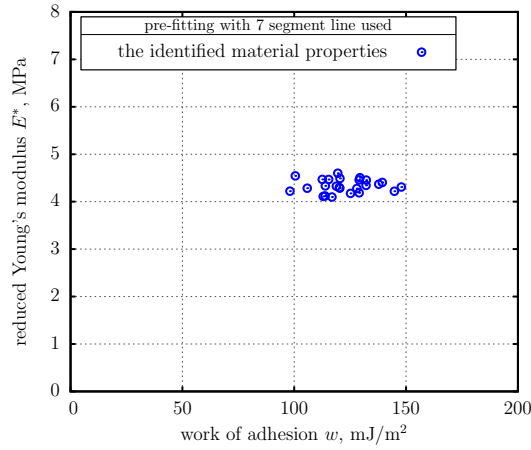
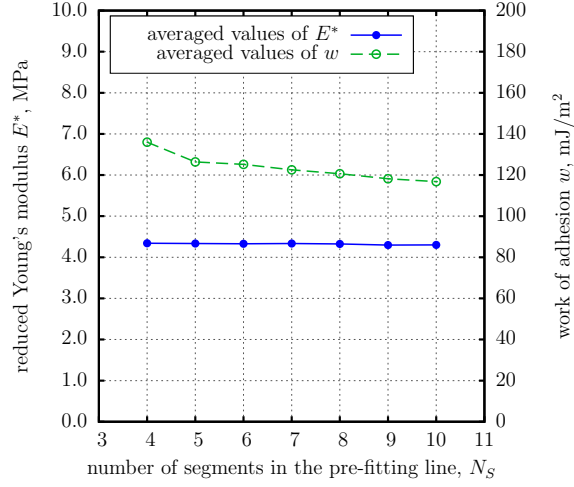


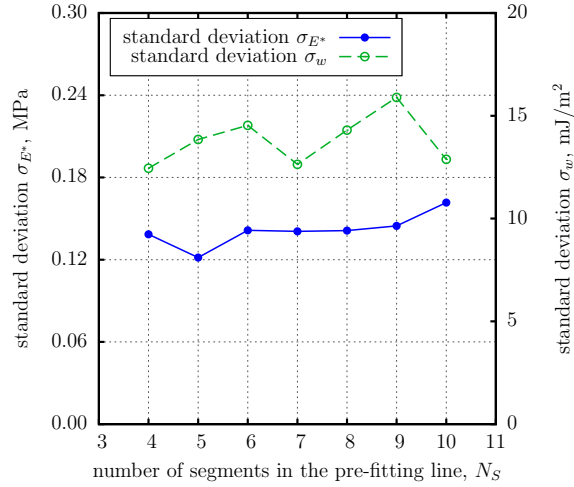
Figure 6: An example of a set of identified values of material properties extracted using pre-fitting with polygonal chain. Number of segments in chain: 7.

The dependency of the averaged values of the reduced elastic contact modulus and the work of adhesion on the number of segments is shown in Fig. 7,a. According to the presented results the averaged values of E^* vary from 4.2959 to 4.3419 MPa, the averaged values of w vary from 0.116 to 0.136 J/m². Clearly, these values do not vary much which shows that the proposed method is stable and robust with respect to chosen number of segments N_S .

The dependency of the values of standard deviation of the reduced elastic contact modulus and the work of adhesion on the number of segments is shown in Fig. 7,b.



(a)



(b)

Figure 7: The experimental results: (a) identified averaged PVS properties values versus the number of segments in the pre-fitting curve (the reduced elastic contact modulus and the work of adhesion), (b) standard deviations of the identified PVS properties values versus the number of segments in the pre-fitting curve.

4. The tensile experiment

The purpose of the tensile test was to validate accuracy of the BG method by evaluation of the reduced elastic contact modulus E^* of the very same PVS material using a completely different experiment, namely a standard tensile test. Since the BG method provided us with the estimated values of the *reduced* elastic modulus, one needs to evaluate both the elastic modulus and Poisson’s ratio from the results of tensile testing, in order to be able to compare the results of these two experiments.

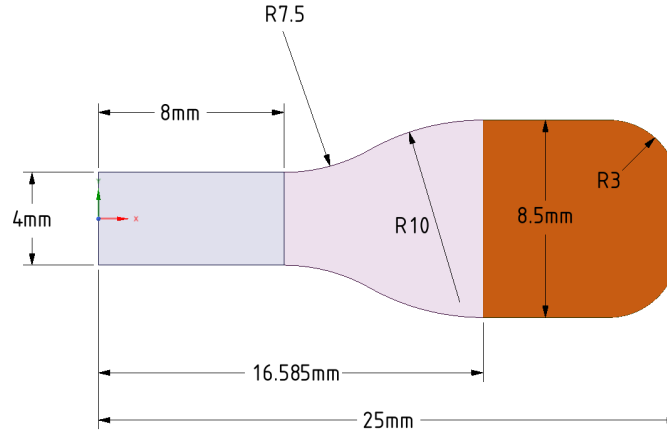
Hence, this Section consists of two independent parts. In the first part we describe the experimental evaluation of the elastic modulus of the PVS, while the second part is devoted to description of the process of estimation of the Poisson’s ratio of the same material using methods of photogrammetry.

4.1. Experimental set-up and the measurements

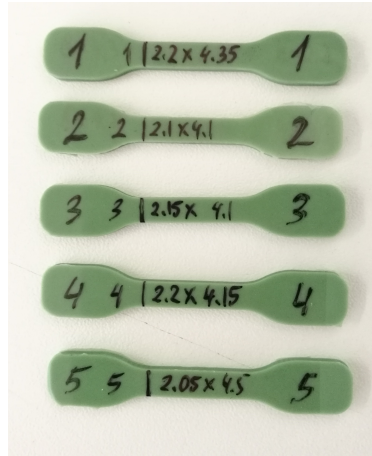
The conventional tensile testing of dumbbell specimens was carried out as an alternative way to determine the properties of PVS (Davis, 2004). The specimens were manufactured as close as possible to the requirements of ISO 37 type 3 specifications and made of exactly the same PVS charge which was used in the DSI testing. The Zwick Roell zwickiLine tensile machine and testXpert II software were employed. A schematic of the specimen is shown in Fig. 8,a. The brown shaded area corresponds to the part of the specimen being gripped by the tensile equipment. Nominal specimen thickness is 2 mm. The five actual specimens had the following dimensions of the cross-sections of the gage sections (thin parts) (thickness x width): 1) 2.2 x 4.35 mm, 2) 2.1 x 4.1 mm, 3) 2.15 x 4.1 mm, 4) 2.2 x 4.15 mm 5) 2.05 x 4.5 mm. The photographic image of the specimens is shown in Fig. 8,b. The specimens were tested approximately 18 h after moulding.

The testing was performed up to 3% of overall grip-to-grip elongation. Each specimen was tested 10 times. The recorded strain-stress curves showed that the specimens 1,3,5 produced very similar results while the two other specimens (2, 4) did not (the two lower sets of lines in Fig. 9,a). These two specimens were considered to have internal defects (most likely these defects were air bubbles inside the material) and were excluded from the further data analysis.

The tests showed that the material behavior may be well described as linearly elastic up to few percent deformation.



(a)



(b)

Figure 8: ISO37 type 3 specimens: (a) the schematic, (b) the actual specimens tested.

The specimens stretching during tensile test was recorded using a HD camera for evaluation of the Poisson's ratio. The methods of photogrammetry were applied to the captured images of the specimens.

The photographic image of the whole set-up is shown in Fig. 9,b.

4.2. Evaluation of elastic modulus. Correction factors for the compliance of the specimens.

Normally, in the tensile experiment the deformation of the thin part (gage section) of the specimen is measured. This allows one to evaluate the elastic

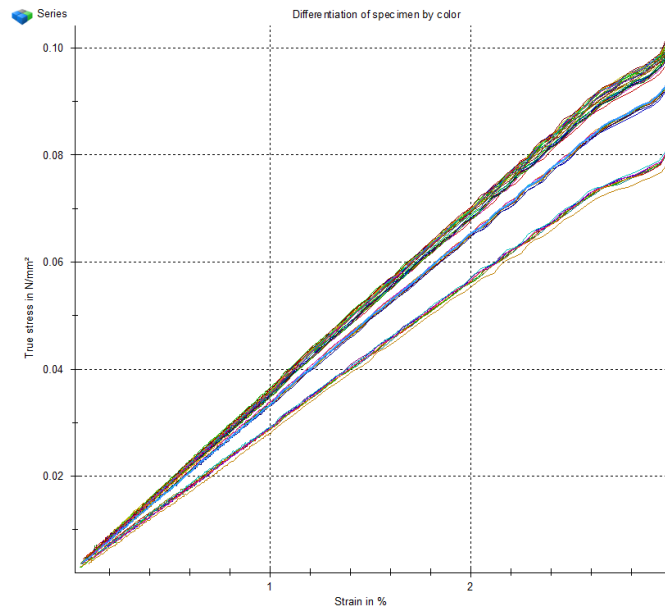
modulus using simplest theory of a rod under uniaxial tension.

Indeed, consider a rod of length L_0 and constant rectangular cross-section of area $A = b_0 \cdot h$ where b_0 is its width and h is the thickness, under tensile load P . Assuming homogeneous uniaxial stress condition inside the rod, the elastic modulus of the material can be determined as

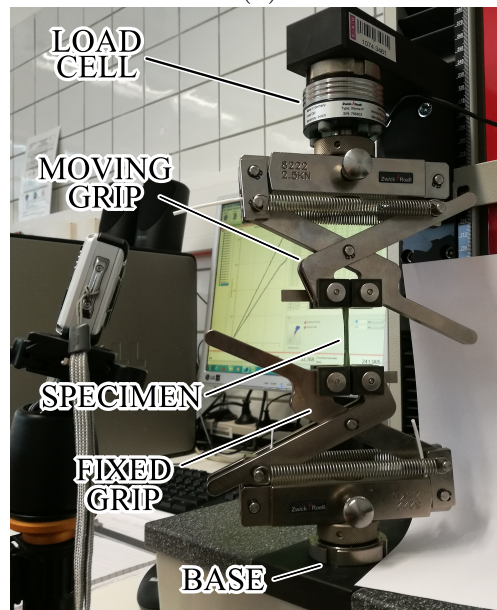
$$E = \frac{d\sigma}{d\varepsilon} = \frac{d\left(\frac{P}{A}\right)}{d\left(\frac{\Delta L_0}{L_0}\right)} = \frac{L_0}{A} \frac{dP}{d\Delta L_0} = \frac{L_0}{b_0 h} \frac{dP}{d\Delta L_0} \quad (20)$$

where ΔL_0 is the elongation of the rod. Assuming linear behaviour of the material, one can also write

$$E = \frac{L_0}{b_0 h} \frac{P}{\Delta L_0}. \quad (21)$$



(a)



(b)

Figure 9: (a) the stress-strain curves for specimens 1-5 (screenshot of the testXpert software), (b) the experimental set-up for the tensile experiment.

Because our experimental set-up was not equipped with an extensometer to control the deformation of the gage section of the specimens, the deformation of the whole specimen was controlled (the grip-to-grip elongation). If the grip-to-grip distance is denoted as L and the grip-to-grip elongation is denoted as ΔL , then simple substitution L as L_0 and elongation of the whole specimen ΔL as ΔL_0 into (21) clearly introduces some amount of inaccuracy because the grip-to-grip elongation is influenced by the compliance of the non-gage parts of the specimen and the machine compliance as well.

It should be noted that many authors argue that shape of specimens and the compliance of the load cell of the tensile machine can influence the results significantly. For example, Jia and Kagan (1999) provide evidences that the results may differ drastically from the expected ones due to the compliance of the dumbbell parts of the specimens and machine compliance. Further, Sergueeva et al. (2009) found that the calculated values of elastic modulus depended on the specimen geometry, in particular, on the gage length of the specimen. Thus, because the specimens were made of rather soft material, the influence of the compliance of the dumbbell parts of the specimens must be assessed and the method for computation of the results corrected.

Load-cell compliance was taken into account during the factory calibration of the Zwick/Roell material testing machine. Therefore, this factor was not considered, only the compliance of the specimen has to be analyzed.

Consider a dumbbell specimen of the length L and constant thickness h which is subjected to tensile load by the force P . The width of the cross-section is the function of the picked location $b(x)$. Let us consider the gage section of the specimen subjected to uniaxial stress. This part has length L_0 and cross-section width b_0 (Fig. 10). In our experiment the grip-to-grip distance was $L = 33.16\text{mm}$ and the gage length was $L_0 = 10\text{mm}$ for ISO37 type 3 specimens. Let us follow the ideas expressed in Jia and Kagan (1999) for estimation of the error introduced into the evaluated value of E when one substitutes L as L_0 and elongation of the whole specimen ΔL as ΔL_0 into (21).

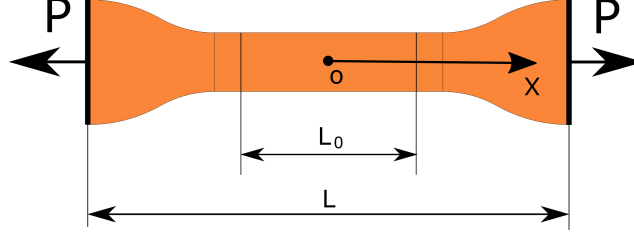


Figure 10: A dumbbell specimen under tension.

Let us denote here by E the true value of elastic modulus and by E_a the *apparent* elastic modulus, where

$$E = \frac{L_0}{b_0 h} \frac{P}{\Delta L_0}, \quad E_a = \frac{L}{b_0 h} \frac{P}{\Delta L}. \quad (22)$$

Consider the value of ΔL in (22) under the hypothesis of uniform stress across the section of the specimen

$$\begin{aligned} \Delta L(P) &= 2 \int_0^{L/2} \varepsilon(x) dx = 2 \int_0^{L/2} \frac{\sigma(x)}{E} dx = \\ &= 2 \int_0^{L/2} \frac{P}{A(x) E} dx = 2 \int_0^{L/2} \frac{P}{E h b(x)} dx = \\ &= \frac{2P}{E h} \int_0^{L/2} \frac{dx}{b(x)}. \end{aligned} \quad (23)$$

Substitution of (23) into (22) yields

$$E_a = \frac{L}{b_0 h} \frac{P}{\Delta L} = \frac{LP}{b_0 h \frac{2P}{E h} \int_0^{L/2} \frac{dx}{b(x)}} = \frac{LE}{2b_0 \int_0^{L/2} \frac{dx}{b(x)}}. \quad (24)$$

The latter gives the value of the correction factor k which is the ratio of apparent to the real elastic moduli:

$$k = \frac{E_a}{E} = \frac{L}{2b_0 \int_0^{L/2} \frac{dx}{b(x)}}. \quad (25)$$

Using the standard dimensions of the ISO37 specimens, the cross-section width $b(x)$ can be expressed (in millimeters) as the following piece-wise function

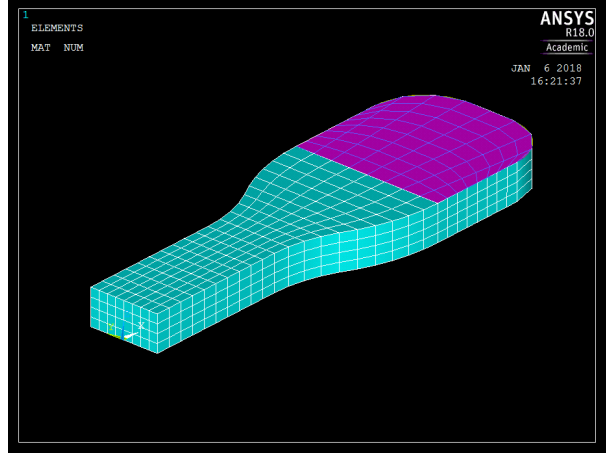
$$b(x) = 2 \begin{cases} 2 & \text{for } x \in [0; 8), \\ 9.5 - \sqrt{7.5^2 - (x - 8)^2} & \text{for } x \in [8; 11.679), \\ -5.75 + \sqrt{10^2 - (x - 16.585)^2} & \text{for } x \in [11.679; 16.585), \\ 4.25 & \text{for } x \geq 16.585. \end{cases} \quad (26)$$

Substitution of this function into (25) gives the value of correction factor as $k = 1.2002$. One can see that according to this rough analytical model, the real elastic modulus may be 20% lower than the apparent one which is rather a significant correction. Therefore, more thorough study is performed below.

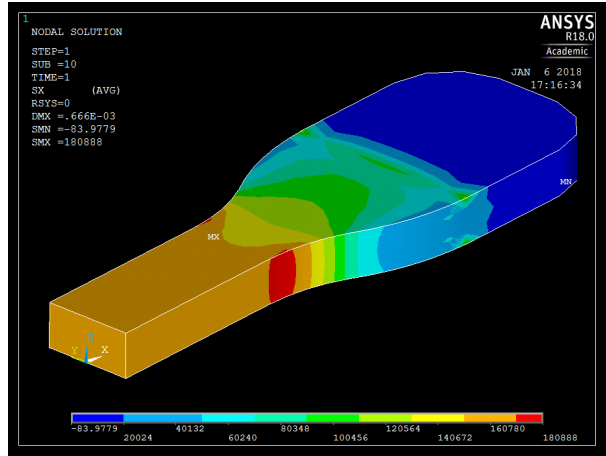
In order to obtain more accurate value of the correction factor k , finite element modeling of the tensile experiment was performed using ANSYS 18 Mechanical APDL software in symmetric formulation (particularly, only the half of the model was built) using the SOLID186 finite element type. The FE model is depicted in Fig. 11,a. The shaded areas were the subject to nodal constraint loading: the nodal displacements UY and UZ were assigned zero values while the nodal displacements UX were assigned the value $UX = \Delta L/2 = 0.03L/2 = 1.33$ mm which is 1.5% of initial grip-to-grip distance. As it was mentioned earlier, the real testing was performed up to the elongation of 3% of the grip-to-grip distance.

Analysis of the stress distribution (Fig. 11,b) shows that this model is more accurate than the previous one since the stress distribution across the cross-section is homogeneous only in the central part of the specimen while the previous analytical model (23) model assumed this across the whole specimen.

Since the stress distribution in the middle part of the specimen can be considered uniaxial, the total applied force was evaluated as $P = \sigma_{x0} \cdot h \cdot b_0$, where σ_{x0} is the stress in the center of symmetry of the whole FE-modeled specimen (point O in Fig. 10).



(a)



(b)

Figure 11: FE modeling of the tensile experiment: (a) the FE model, (b) the distribution of the σ_x stresses in the specimen.

Since ANSYS applies loads gradually via several sub-steps, it was possible to evaluate the apparent elastic modulus using differential formula as

$$E_a = \frac{L}{b_0 h} \frac{dP}{d\Delta L}. \quad (27)$$

Differential formula allowed us to track changes in E_a with respect to model deformation (if any). Differentiation was performed numerically by means of ANSYS itself. Since the "true" value of E was set in the beginning of the simulation, the correction factor was computed as $k = E_a/E$.

Multiple trial runs under different parameter values showed that in linear formulation the coefficient k : (i) does not depend on the values of E in the wide range of applied stresses (1-6 MPa), (ii) slightly depends on Poisson's ratio (for a large interval of the ratio values $\nu = 0.2...0.49$, it may change approximately by 0.017), (iii) depends on specimen geometry and, in particular, for the standard ISO37 type 3 specimen made of a material with $\nu = 0.417$ it is equal to $k = 1.16977$, (iv) does not depend on specimen deformation in linear FE formulation.

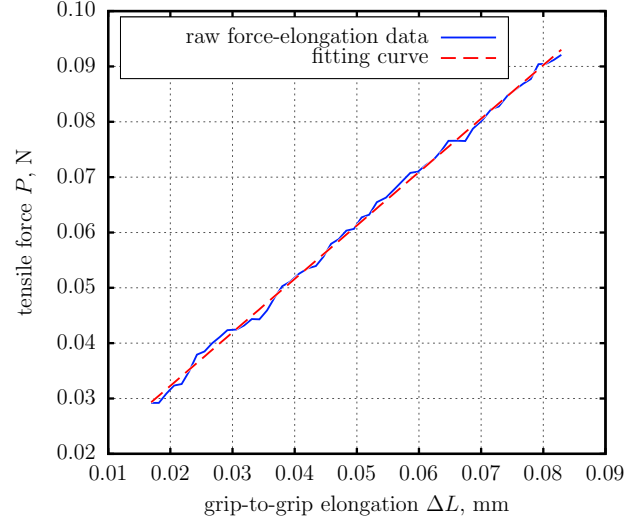
Individual values of the correction coefficients k obtained by means of ANSYS for the specimens No. 1, 3 and 5 were the following: $k_1 = 1.15294$, $k_3 = 1.16338$, $k_5 = 1.14864$.

The latter coefficients allowed us to evaluate the values of E from experimental data using the following strategy. First, for each of the three specimens and each of 10 tests per specimen, the force-elongation dependency was fitted with straight line in the interval $\frac{\Delta L}{L} \in [0.0005; 0.0025]$ and the value $\frac{dP}{d\Delta L}$ was found. Note that fitting by means of linear regression was needed because the data was rather noisy when deformations were very small (Fig. 12,a).

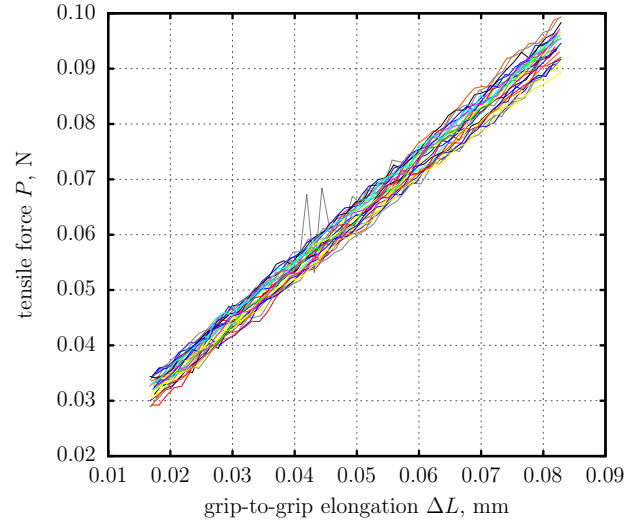
Then the apparent value of elastic modulus was evaluated using (27). The true values of E were calculated as $E = \frac{E_a}{k}$ using individual correction coefficients. Finally, the whole 30 values of E were statistically post-processed.

The raw force-elongation dependencies obtained during the experiment in the interval $\frac{\Delta L}{L} \in [0.0005; 0.0025]$ are shown in Fig. 12,b.

The computed values of the elastic modulus versus the test number for all the three specimens are presented in Fig. 13. The averaged value across all 30 data sets is $\langle E \rangle = 2.9723$ MPa. Standard deviation of the obtained data is $7.3833e-2$ MPa.



(a)



(b)

Figure 12: Force-elongation dependencies obtained during the experiment in the interval $\frac{\Delta L}{L} \in [0.0005; 0.0025]$ (raw data): (a) fitting the raw data with a straight line, (b) the raw force-elongation data for all 3 valid specimens (10 measurements per specimen).

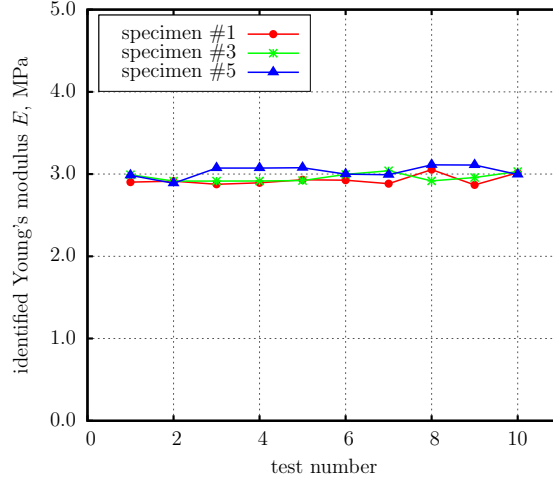


Figure 13: The computed values of the elastic modulus versus the test number. Dots: specimen 1, asterisks: specimen 3, triangles: specimen 5.

Obtaining the value of elastic modulus is not enough to validate the results of the DSI experiment in this study. In order to do so, evaluation of the Poisson's ratio of the PVS is required. The corresponding method is discussed below.

4.3. Estimation of Poisson's ratio

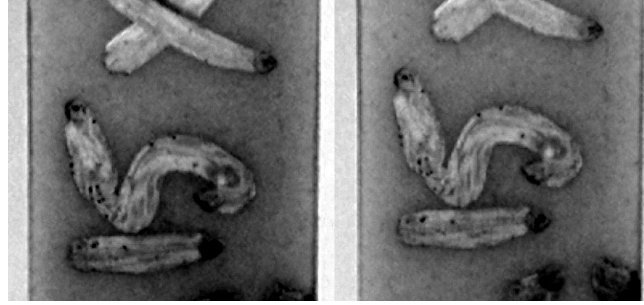
In order to estimate Poisson's ratio of the PVS, the photogrammetry approach was used that allowed us to capture the necessary data from the tensile experiments. In particular, video recording of the stretching process of the specimens was performed using a camera with HD resolution in the macro mode using different magnification factors. By extracting the photographic image of the specimen before and after stretching, it is possible to estimate the deformations in axial direction ε_x and in orthogonal direction ε_y . Poisson's ratio may be then evaluated as $\nu = -\frac{\varepsilon_y}{\varepsilon_x}$.

In the beginning all recorded videos were subject to temporal denoising and then pairs of images (before/after stretching) were extracted. These images were converted to HSV colour system and only the "Value" (V) channel was kept producing grayscale pairs of specimens' photographs. Using Matlab the contrast of these pairs of grayscale images was enhanced using the *imadjust* routine and the images were also sharpened using the *imsharpen* routine. The examples of such pairs of post-processed images are shown in

Fig. 14. In total, 17 image pairs of this kind were produced. Two of such image pairs are shown in the Fig. 14. In each pair, the top/left image corresponds to the undeformed specimen, while the bottom/right one corresponds to the stretched specimen.



(a)



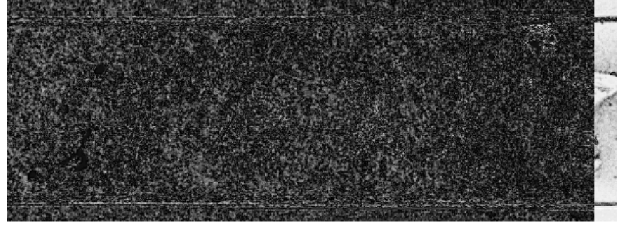
(b)

Figure 14: Examples of post-processed images used for identification of the specimens' deformations (in each pair: the top/left one is before and the bottom/right one is after stretching): (a) the images taken at low magnification, (b) images taken at high magnification.

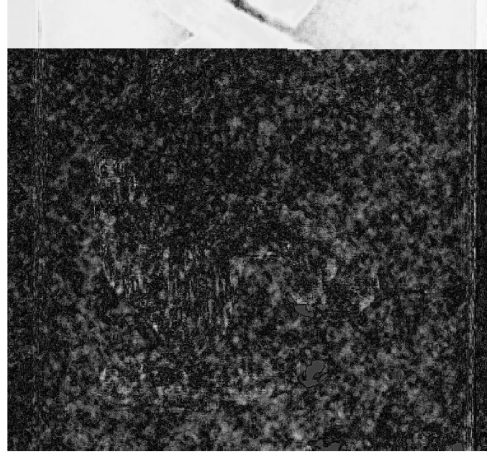
Next, the Matlab routine *imregtform* was applied to each pair of images producing a global affine transform necessary to fit the image of the stretched specimen into the initial photograph of that specimen. For this purpose, in each pair one of the images was kept unchanged while the second one was deformed (including shift, shear, stretching and rotation) so that finally it became a part of the first image (or they had some parts in common). This is the so-called image registration process.

In order to assure the quality of performed image registration, the differ-

ence between the images was computed for each pair. In a pair of grayscale images each one is essentially a matrix with integer values in 0..255 range. Hence, the difference image is a matrix containing the absolute values of the result of their subtraction. If some features in the two images coincide, the dark area on the difference image is produced. Only the features that do not coincide are highlighted because they have a non-zero difference in the luminosity values. Examples of such difference images corresponding to Fig. 14 are shown in Fig. 15. It can be noted that the difference images contain only noise and do not contain the features of the original images which is a good evidence of successful registration. That is, the affine transform allowing to fit the right image into the left one was computed with high accuracy. More on digital image processing methods can be found in Gonzalez and Woods (2018) and the corresponding sections of Matlab manual.



(a)



(b)

Figure 15: Examples of difference images produced for image pairs after registration. There are no features of the original images in the regions where subtraction was performed which is the sign of successful registration. The brightness is increased for illustrative purpose.

Next, the above mentioned affine transform was inverted producing the transform from initial to stretched state. The produced affine transform contains information about translation, rotation, axial and shear deformations necessary to fit one image into another. Since image registration via *imregtform* was performed iteratively as the result of Matlab's internal optimization algorithm, the obtained transforms did not purely contain axial deformations but also small amount of the other types of transformation. In order to extract the information about axial deformations in vertical and horizontal directions it was decided to apply the obtained transform to a set of points with known coordinates initially forming a square (Fig.16,a). Let a be the side length of this square.

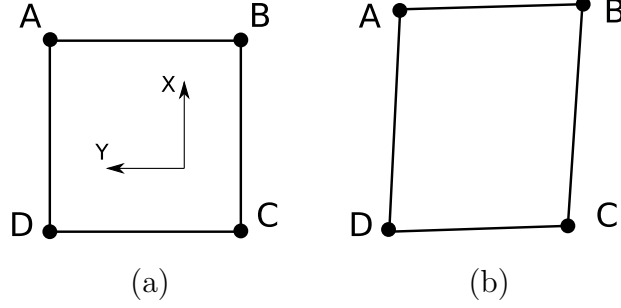


Figure 16: Set of four points forming a quadrangle before and after application of the identified affine transform: (a) initial state, (b) deformed state. The amount of shear deformation is increased for illustrative purpose.

After evaluation of the coordinates of the vertices of the deformed square the absolute values of axial deformations were estimated as follows

$$\begin{aligned}\varepsilon_x &= \frac{\frac{|x_A - x_D| + |x_B - x_C|}{2} - a}{a}, \\ \varepsilon_y &= \frac{\frac{|y_A - y_B| + |y_D - y_C|}{2} - a}{a}.\end{aligned}\tag{28}$$

Finally, Poisson's ratio was computed as

$$\nu = -\frac{\varepsilon_y}{\varepsilon_x}.\tag{29}$$

The results of evaluation of Poisson's ratio values for all 17 image pairs is represented in Fig. 17. The averaged value is $\nu = 0.41758$, the standard deviation is $\sigma_\nu = 0.0147$.

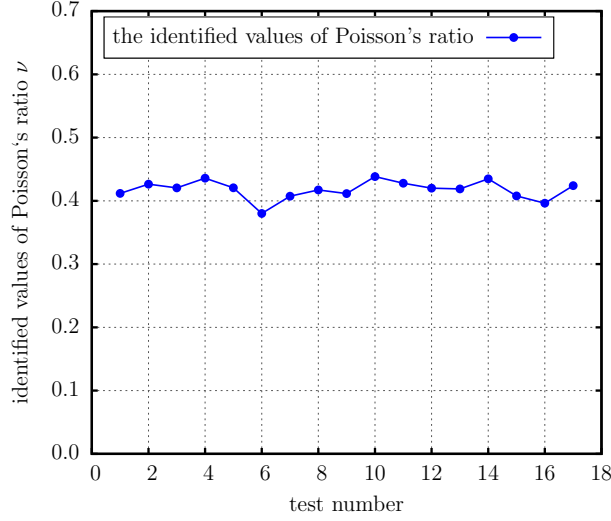


Figure 17: The computed values of the Poisson's ratio for different captured images.

5. Comparison of the results of two experiments

Now the results of the two different experiments can be compared. As it has been discussed above, the experimental results are influenced by many factors related to the used equipment, mathematical algorithms, and assumptions of different kinds. Let us analyse briefly some of these factors.

Two types of noise were present in the measured DSI data: high-frequency noise and small low-frequency fluctuations that influenced the overall trend of load-displacement curves. The noise was produced mostly from the electronic circuits of the DSI sensors and was effectively eliminated by the pre-fitting curve. Slow fluctuations in the data can be caused by small inhomogeneities of properties of the surface of the specimen. Influence of these factors was minimized by multiple repeated testing at different locations. A pre-fitting curve with the low number of degrees of freedom may also smooth away 'bumps' in the measured load-displacement sequence.

The experimental results showed in Fig. A.19-A.20 are packed in rather tight clouds of points which demonstrate the robustness and accuracy of the tested BG approach. However, the optimal number of segments in the pre-fitting polygonal chain may be the matter of discussion because the obtained results do not exhibit a clearly visible optimum, e.g. global minimum in standard deviation etc., and low number of segments leads to unreason-

able increase in the identified values of the work of adhesion. In any case, the results corresponding to different numbers of segments in the pre-fitting polygonal chain do not differ significantly.

In the DSI experiment we used the JKR theory of adhesive contact as the theoretical background. This theory requires the tested elastic medium to be a half-space. Using numerical simulations, we showed in the corresponding Section that the thick PVS specimen effectively models properties of an elastic half-space, given that indentation depth is small. However, the finite size specimen is stiffer than a half-space which means that the actual measured values of indentation force were slightly higher than it would be expected. The same effect may also be caused by non-linearity of the constitutive law for PVS. As PVS is a hyperelastic material, it means that non-linear components of stresses - however small they might be - make the specimen material appear stiffer during compression in comparison to purely linear case or in comparison to tensile load.

Altogether, the above means that the values of the reduced elastic contact modulus E^* obtained by means of the BG method using that particular specimen are slightly higher than they could be if the BG method was applied to a data obtained using a linearly elastic half-space.

On the other hand, the tensile experiment has its own sources of possible inaccuracies. It can be seen that at small deformation range (at which elastic modulus is usually identified) the obtained force-elongation data is rather noisy (Fig. 12). This issue has been overcome by means of fitting the data with straight line. Normally, the obtained values of both the force and elongation are used in conventional formulae of the materials science describing a rod under tension which allows to estimate the value of the elastic modulus quite easily.

Clearly, it was not the case in our experiment because the elongation of the gage section of the specimens could not be measured directly and the deformation of the whole specimen was measured instead. Therefore, we studied how the identified values of elastic modulus depend on the compliance of the non-gage parts of the sample. Both analytical and numerical modeling provided similar values of the correction factor k (the ratio of the apparent to the real elastic moduli). Similarity of these results obtained in different ways indicates that the obtained value of the correction factor is rather correct.

Finite element model indeed provided more accurate values of k since it better reproduced stress distribution in the specimen. However, the presence of grip force was not taken into account in it. It is expected that if grip

pressure is applied to the grip area in the FE model (shaded areas in Fig. 8,a and Fig. 11,a) instead of zero normal displacements, it causes reduction in the tension of the gage section as material is "squeezed" out of the grip. In turn, this should reduce the computed correction factors k . Thus, the real identified values of the elastic modulus of the PVS are likely to be a little higher than the presented in the previous Section because they were calculated as $E = E_a/k$.

Poisson's ratio of the PVS in this work was not determined from a separate dedicated experiment but rather estimated using photogrammetry approaches. Simple determination of deformations using changes in distance between features in specimens' photographs might be an unreliable approach when processing images containing noise. Hence, we applied ready-to-use Matlab routines for image registration which computed a global transform needed to fit the photograph of the stretched specimen into the photograph of the unstretched one. In this case the entire image was used as the source of metric calculation for image fitting algorithm. As the result, the obtained estimated values of Poisson's ratio looked pretty stable with respect to different zoom factors used and different amounts of noise present in the processed images. This is an implicit evidence of the correctness of the obtained results. It also should be noted here that PVS is a rubber-like material. So we expect that in case of any inaccuracies the real values of Poisson's ration should not be less than the identified value $\nu = 0.41758$ but even higher than that. In that case, the value of E^* identified in the tensile experiment should also be higher.

Applying the extended BG method to the results of the DSI tests, the values of the reduced elastic contact modulus E^* and the work of adhesion w of the tested material were obtained. The averaged values of E^* varied from 4.2959 to 4.3419 MPa, while the averaged values of w varied from 0.116 to 0.136 J/m² depending on the number of segments in the pre-fitting line. Indeed, the identified values of the reduced contact modulus and the work of adhesion depend on the theory of adhesive contact used as the mathematical model for the indentation experiment. Hence, the use of the JKR theory as the framework for the problem must be justified.

In their papers Tabor (1977) and Muller et al. (1980) (see also Maugis (2000)) introduced a dimensionless parameter suitable for clear distinction of applicability range between the JKR and the DMT theories of adhesive contact:

$$\mu = \left(\frac{Rw^2}{E^{*2}z_0^3} \right)^{1/3} \quad (30)$$

where R is the effective curvature radius of contacting bodies (if a sphere is in contact with a plane, R is equal to the radius of the sphere, that is $R = 5.155$ mm); z_0 is the equilibrium distance between atoms of the contacting bodies, usually assumed to be 0.3...0.5 nm.

Values $\mu \gg 1$ indicate that the experiment is in the applicability range of the JKR theory, while values $\mu \ll 1$ suggest that the DMT theory should be used. Assuming $z_0 = 0.4$ nm and using the total maximum and minimum identified values of E^* and w among all calculations (see Table 1 and 2 below) one can estimate the range of values of the parameter μ as follows:

$$\mu_{min} = \left(\frac{Rw_{min}^2}{E_{max}^{*2}z_0^3} \right)^{1/3}$$

and

$$\mu_{max} = \left(\frac{Rw_{max}^2}{E_{min}^{*2}z_0^3} \right)^{1/3}$$

where the subscripts "max" and "min" denote the maximum and the minimum identified values of the corresponding physical quantities.

The calculated values of the Tabor-Muller parameters were: $\mu_{min} = 2930.2$, $\mu_{max} = 5014.1$. Thus, the DSI tests in the present work fall within the range of applicability of the JKR theory.

In the second experiment, tensile testing of dumbbell PVS specimens was performed. The obtained data allowed us to evaluate the values of elastic modulus and Poisson's ratio of the material of the specimens. The corresponding values were $E = 2.9723$ MPa (averaged across the set of 30 values with minimum identified value of 2.8687 MPa and maximum identified value of 3.1121 MPa) and $\nu = 0.41758$ (averaged across the set of 17 values with minimum identified value of 0.37999 and maximum identified value of 0.43827) which gave us the value of the estimate value of the reduced elastic contact modulus as $E^* = E/(1 - \nu^2) = 3.60005$ MPa. Using the above minimum and maximum values of E and ν one can find that the lowest and the highest individual identified values of the reduced elastic contact modulus E^* in the tensile experiment were 3.353 MPa and 3.852 MPa respectively.

Table 1 contains minimum, maximum, and averaged values of the reduced elastic contact modulus E^* identified by means of the BG method from the

DSI experiment (depending on the number of segments N_S in pre-fitting line). The relative differences with the tensile experiment (based on mean values) are shown as well. The relative differences Δ_{rel} in the identified values were computed as

$$\Delta_{rel} = \frac{|E_{TENS}^* - E_{DSI}^*|}{E_{DSI}^*} \quad (31)$$

where E_{TENS}^* and E_{DSI}^* are the values identified from the tensile experiment and in the DSI experiment (by means of the BG method) respectively.

Graphical comparison of the results of the two experiments (identification of E^*) is shown in Fig. 18. Filled rectangles denote total ranges of individual identified values of E^* in all calculations. Dots denote averaged values of E^* . Percentages denote relative difference in values calculated according to (31). In case of the DSI experiment the BG method was used. Hence, multiple dots correspond to different values of N_S in pre-fitting.

Detailed comparison of the values of E^* calculated in the two experiments (Fig. 18) showed that the relative difference (31) between total maximum in the tensile experiment and the total minimum in the DSI experiment was 3.80%. The relative difference between total minimum in the tensile experiment and the total maximum in the DSI experiment was 27.38%. The relative difference in averaged values of E^* varied between 16.20% and 17.09% depending on the number of segments N_S used during pre-fitting. This can be considered as a good result.

Summarizing all the above considerations, we note that due to the sample size effect and the material properties the values of E^* identified by means of the BG method were slightly higher than they could have been. At the same time, due to shortcomings in the processing of the data of the tensile experiment the identified values of E^* were lower than they could be. Thus, the difference in results of the two experiments could be even smaller than the figures of 16.20 ... 17.09% stated above. Thus, the accuracy of the extended BG method in formulation (16) has been directly confirmed.

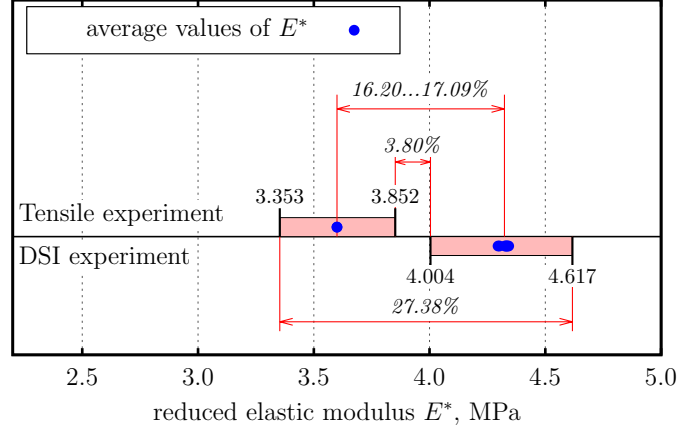


Figure 18: Graphical comparison of the results of the two experiments (identification of E^*). Filled rectangles: total ranges of individual identified values of E^* in all calculations; dots: averaged values; percentages denote relative differences (31). In case of the DSI experiment the BG method was used. Hence, multiple dots correspond to different values of N_S in pre-fitting.

Table 1: Minimum, maximum, averaged values of the reduced elastic contact modulus E^* identified by means of the BG method, and the relative difference from the results of the tensile experiment $\Delta_{rel.avg}$ for averaged values versus the number of segments N_S in pre-fitting line.

N_S	min E^* , MPa	max E^* , MPa	avg E^* , MPa	$\Delta_{rel.avg}$, %
4	4.004	4.544	4.342	17.09
5	4.131	4.558	4.336	16.97
6	4.027	4.541	4.329	16.84
7	4.099	4.599	4.334	16.93
8	4.051	4.586	4.325	16.76
9	4.065	4.609	4.296	16.20
10	4.064	4.617	4.302	16.32

Table 2: Minimum, maximum, averaged values of the work of adhesion w identified by means of the BG method versus the number of segments N_S in pre-fitting line.

N_S	min w , J/m ²	max w , J/m ²	avg w , J/m ²
4	0.1042	0.1584	0.1360
5	0.1022	0.1536	0.1264
6	0.0832	0.1468	0.1252
7	0.0981	0.1479	0.1226
8	0.0816	0.1555	0.1207
9	0.0879	0.1489	0.1182
10	0.0966	0.1476	0.1168

Conclusions

In this work a concept of a model-based approach to simultaneous identification of elastic (the reduced elastic contact modulus E^*) and adhesive (the work of adhesion w) properties of materials and structures from experimental results of depth sensing indentation (DSI) has been presented. This new approach is an extended version of the BG method developed by Borodich and Galanov (2008) which uses different objective functional and the idea of preliminary smoothing the data.

The extended BG method uses the concept of two-stage fitting of the theoretical DSI dependency to the experimental data points. Firstly, the data is fitted with an auxiliary curve which acts as a filter in certain sense. The mathematical representation of this pre-fitting curve is supposed to be as simple as possible. This allows us to use some advanced fitting/filtering techniques to reduce measurement noise and fluctuations in the data. Secondly, the theoretical load-displacement curve (the expected DSI dependency which may be a complex expression) is fitted to the auxiliary one via minimization of the squared norm of the difference of the two functions (the objective functional). The sought material properties are determined from the optimal set of characteristic parameters that give minimum to the objective functional.

The accuracy and robustness of the above approach has been directly validated by means of two independent experiments in which the properties of specimens made of polyvinyl siloxane (PVS) were determined. Both experiments allowed us to evaluate the values of the reduced elastic modulus E^* of the PVS and compare these values.

In the first experiment a DSI equipment was used and the BG method

was applied to the obtained data as described above using the JKR theory of adhesive contact as the theoretical background for the problem. The pre-fitting curve was chosen to be a polygonal chain. It was fitted to the normalized (dimensionless) data using orthogonal distance fitting approach which has advantage over conventional least-squares fitting when both force and displacement readings are supposed to have measurement errors.

In the second experiment we performed tensile testing of dumbbell PVS specimens while taking video recording of the stretching process. The obtained data allowed us to separately evaluate the values of elastic modulus and Poisson's ratio of the material of the specimens and then calculate the value of the reduced elastic modulus of the material.

Comparison of the of the results of the two experiments showed that the absolute minimum in relative difference between individual identified values of the reduced elastic modulus E^* in the two experiments was 3.80%; the absolute maximum of the same quantity was 27.38%; the relative difference in averaged values of E^* varied between 16.20% and 17.09% depending on the number of segments N_S used during pre-fitting. The above can be considered as a good result. Our analysis showed that unaccounted factors and phenomena tend to decrease the differences in the results of the two experiments. Therefore, the results obtained by means of the two different methods in this work should differ even less.

However, since the results of the two experiments coincide well enough, it can be concluded that the methods used in both experiments are rather effective and well justified as well as the used assumptions. Thus, the robustness and accuracy of the proposed extension of the BG method has been directly validated.

Acknowledgements

This collaborative work between Cardiff University, UK and Christian-Albrechts-Universität zu Kiel, Germany was initiated as a part of activities of the CARBTRIB International Network supported by the Leverhulme Trust. The authors are grateful to the Leverhulme Trust for the support of their collaboration.

The visits of Prof. Feodor Borodich and Dr. Nikolay Perepelkin to the Functional Morphology and Biomechanics Group at Kiel University were supported by Alexander von Humboldt Foundation and the European Union's

Horizon 2020 research and innovation programme under the Marie Skłodowska-Curie grant agreement No 663830 respectively. Thanks are due to Alexander von Humboldt Foundation and the Marie Skłodowska-Curie programme.

References

- Ahn, S. J., 2004. Least Squares Orthogonal Distance Fitting of Curves and Surfaces in Space. Springer-Verlag, Berlin.
- Al-Musawi, R. S., Brousseau, E. B., Geng, Y., Borodich, F. M., 2016. Insight into mechanics of afm tip-based nanomachining: bending of cantilevers and machined grooves. *Nanotechnology*. 27, 385302.
- Argatov, I. I., Borodich, F. M., Epshtein, S. A., Kossovich, E. L., 2017. Understanding of material properties of thin films attached to substrates: depth-sensing unloading of elasto-plastic and elasto-brittle materials. *Mech. Mater.* 114, 172–179.
- Beach, E. R., Tormoen, G. W., Drelich, J., Han, R., 2002. Pull-off force measurements between rough surfaces by atomic force microscopy. *J. Colloid Interface Sci.* 247 (1), 84–99.
- Boggs, P. T., Byrd, R. H., Schnabel, R. B., 1987. A stable and efficient algorithm for nonlinear orthogonal distance regression. *SIAM J. Sci. Stat. Comput.* 8 (6), 1052–1078.
- Borodich, F. M., 2014. The Hertz-type and adhesive contact problems for depth-sensing indentation. *Adv. App. Mech.* 47, 225–366.
- Borodich, F. M., Galanov, B. A., 2008. Non-direct estimations of adhesive and elastic properties of materials by depth-sensing indentation. *Proc. R. Soc. Ser. A*. 464, 2759–2776.
- Borodich, F. M., Galanov, B. A., Gorb, S. N., Prostov, M. Y., Prostov, Y. I., Suarez-Alvarez, M. M., 2012a. Evaluation of adhesive and elastic properties of materials by depth-sensing indentation of spheres. *J. App. Phys. A: Mater. Sci. and Processing*. 108 (1), 13–18.
- Borodich, F. M., Galanov, B. A., Gorb, S. N., Prostov, M. Y., Prostov, Y. I., Suarez-Alvarez, M. M., 2012b. An inverse problem for adhesive contact

- and non-direct evaluation of material properties for nanomechanics applications. *Nanoscale Systems: Mathematical Modeling, Theory and Applications*. 1, 80–92.
- Borodich, F. M., Galanov, B. A., Gorb, S. N., Prostov, M. Y., Prostov, Y. I., Suarez-Alvarez, M. M., 2013. Evaluation of adhesive and elastic properties of polymers by the bg method. *Macromol. React. Eng.* 7, 555–563.
- Borodich, F. M., Keer, L. M., 2004a. Contact problems and depth-sensing nanoindentation for frictionless and frictional boundary conditions. *Int. J. Solids Struct.* 41, 2479–2499.
- Borodich, F. M., Keer, L. M., 2004b. Evaluation of elastic modulus of materials by adhesive (no-slip) nanoindentation. *Proc. R. Soc. Ser. A*. 460, 507–514.
- Boyd, S., Vandenberghe, L., 2004. *Convex Optimization*. Cambridge Univ. Press.
- Bull, S. J., 2005. Nanoindentation of coatings. *J. Phys. D: App. Physics*. 38, 393–413.
- Bulychev, S. I., Alekhin, V. P., Shorshorov, M. K., Ternovskii, A. P., Shnyrev, G. D., 1975. Determination of young’s modulus according to indentation diagram (in Russian). *Industrial Laboratory* 41, 1409–1412.
- Bulychev, S. I., Alekhin, V. P., Shorshorov, M. K., Ternovskii, A. P., Shnyrev, G. D., 1976. Mechanical properties of materials studied from kinetic diagrams of load versus depth of impression during microimpression (in Russian). *Strength of Materials*. 8, 1084–1089.
- Carrillo, F., Gupta, S., Balooch, M., Marshall, S., Marshall, G., Pruitt, L., Puttlitz, C., 2005. Nanoindentation of polydimethylsiloxane elastomers: Effect of crosslinking, work of adhesion, and fluid environment on elastic modulus. *J. Mater. Research*. 20 (10), 2820–2830.
- Chai, J., Takahashi, Y., Lautenschlager, E. P., 1998. Clinically relevant mechanical properties of elastomeric impression materials. *Int. J. Prosthodont.* 11, 219–223.

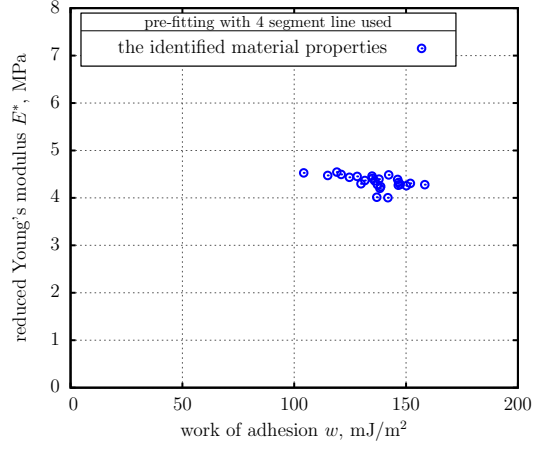
- Chaudhri, M. M., Lim, Y. Y., 2007. Nanoindentation techniques: A critical assessment of the current methods of data analysis. *Key Engineering Materials*. 345-346, 1107–1114.
- Chong, E., Zak, S., 2001. *An introduction to optimization*. Wiley, New York.
- Davis, J. R., 2004. *Tensile Testing* (2nd Ed.). ASM International.
- Derjaguin, B. V., Muller, V. M., Toporov, Y. P., 1975. Effect of contact deformations on adhesion of particles. *J. Colloid Interface Sci.* 53, 314–326.
- Doerner, M. F., Nix, W. D., 1986. A method for interpreting the data from depth-sensing indentation instruments. *J. Mater. Research*. 1, 601–609.
- Ebenstein, D. M., Wahl, K. J., 2006. A comparison of JKR-based methods to analyze quasi-static and dynamic indentation force curves. *J. Colloid Interface Sci.* 298, 652–662.
- Galanov, B. A., Dub, S. N., 2017. Critical comments to the Oliver–Pharr measurement technique of hardness and elastic modulus by instrumented indentations and refinement of its basic relations. *J. Superhard Mater.* 39 (6), 373–389.
- Galanov, B. A., Grigor’ev, O. N., Mil’man, Y. V., Ragozin, I. P., 1983. Determination of the hardness and Young’s modulus from the depth of penetration of a pyramidal indenter. *Strength of Materials*. 15, 1624–1628.
- Galanov, B. A., Grigor’ev, O. N., Mil’man, Y. V., Ragozin, I. P., Trefilov, V. I., 1984. Determination of the hardness and Young’s modulus with elastoplastic penetration of indentors into materials. *Sov. Phys. Dokl.* 29, 146–147.
- Gonzalez, R. C., Woods, R. E., 2018. *Digital Image Processing* (4th Ed.). Pearson Education Inc.
- Gorb, E. V., Gorb, S. N., 2009. IUTAM Symposium on Scaling in Solid Mechanics. Springer, Dordrecht, Ch. Contact Mechanics at the Insect-Plant Interface: How Do Insects Stick and How Do Plants Prevent This?, pp. 243–252.

- Grierson, D. S., Flater, E. E., Carpick, R. W., 2005. Accounting for the JKR–DMT transition in adhesion and friction measurements with atomic force microscopy. *Journal of Adhesion Science and Technology*. 19, 291–311.
- Jia, N., Kagan, V. A., 1999. Limitations of Test Methods for Plastics, ASTM STP 1369. American Society for Testing and Materials, West Conshohocken, PA, Ch. Interpretations of Tensile Properties of Polyamide 6 and PET Based Thermoplastics Using ASTM and ISO Procedures, available at <http://www8.basf.us//PLASTICSWEB/displayanyfile?id=0901a5e180004890>.
- Johnson, K. L., 1985. *Contact Mechanics*. Cambridge University Press, Cambridge.
- Johnson, K. L., Kendall, K., Roberts, A. D., 1971. Surface energy and the contact of elastic solids. *Proc. R. Soc. Lond. A*. 324, 301–313.
- Kalei, G. N., 1968. Some results of microhardness test using the depth of impression (in Russian). *Mashinovedenie*. 4 (3), 105–107.
- Maugis, D., 2000. *Contact, Adhesion and Rupture of Elastic Solids*. Springer-Verlag, Berlin.
- Muller, V. M., Yushchenko, V. S., Derjaguin, B. V., 1980. On the influence of molecular forces on the deformation of an elastic sphere and its sticking to a rigid plane. *J. Colloid Interface Sci.* 77 (1), 91–101.
- Oliver, W. C., Pharr, G. M., 1992. Improved technique for determining hardness and elastic modulus using load and displacement sensing indentation experiments. *J. Mater. Research*. 7, 1564–1580.
- Popov, V. L., 2010. *Contact mechanics and friction*. Springer, Heidelberg.
- Rundlöf, M., Karlsson, M., Wågberg, L., Poptoshev, E., Rutland, M., Claesson, P., 2000. Application of the JKR method to the measurement of adhesion to Langmuir-Blodgett cellulose surfaces. *J. Colloid Interface Sci.* 230 (2), 441–447.
- Sadeghipour, K., Chen, W., Baran, G., 1994. Spherical micro-indentation process of polymer-based materials: a finite element study. *J. Phys. D: Appl. Phys.* 27, 1300–1310.

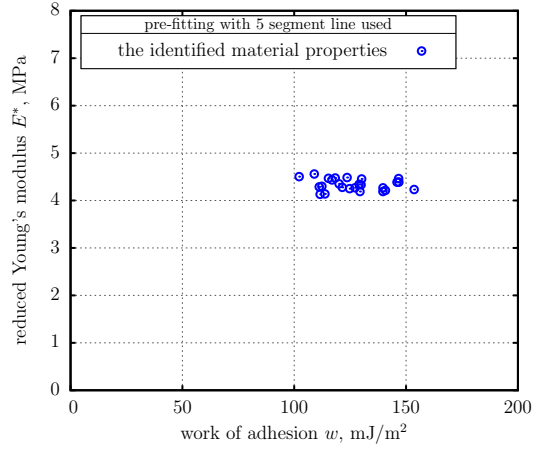
- Sergueeva, A. V., Zhou, J., Meacham, B. E., Branagan, D. J., 2009. Gage length and sample size effect on measured properties during tensile testing. *Materials Science and Engineering: A*. 526 (1), 79–83.
- Shorshorov, M. K., Bulychev, S. I., Alekhin, V. P., 1981. Work of plastic and elastic deformation during indenter indentation (in Russian). *Soviet Physics - Doklady*. 26, 769–771.
- Tabor, D., 1977. Surface forces and surface interactions. *J. Colloid Interface Sci*. 58 (1), 2–13.
- Wahl, K. J., Asif, S. A. S., Greenwood, J. A., Johnson, K. L., 2006. Oscillating adhesive contacts between micron-scale tips and compliant polymers. *J. Colloid Interface Sci*. 296, 178–188.
- Wieckiewicz, M., Grychowska, N., Zietek, M., Wieckiewicz, W., 2016. Evaluation of the elastic properties of thirteen silicone interocclusal recording materials. *BioMed Research International*. 2016, 7456046.
- Yu, Y., Sanchez, D., Lu, N., 2015. Work of adhesion/separation between soft elastomers of different mixing ratios. *J. Mater. Research*. 30 (18), 2702–2712.

Appendix A. The results of application of the BG method (complete set)

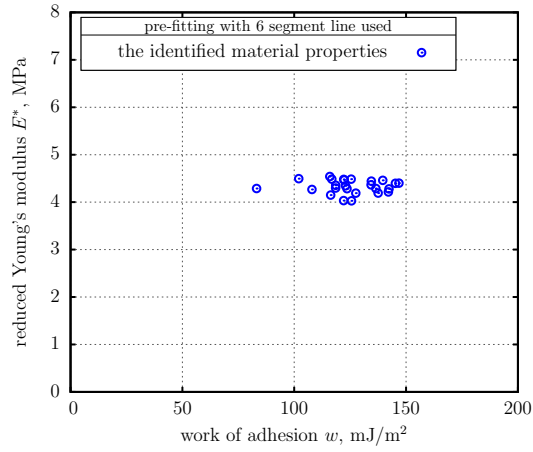
In the following figures the results of identification of the PVS properties are shown as the number of segments in the pre-fitting polygonal chain varies from 4 to 10. The values of E^* and w were identified separately for each of the 25 data sets. The result of each identification is represented as a dot in the figures.



(a)

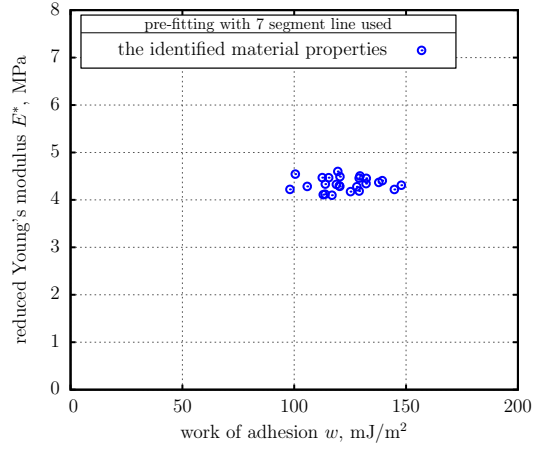


(b)

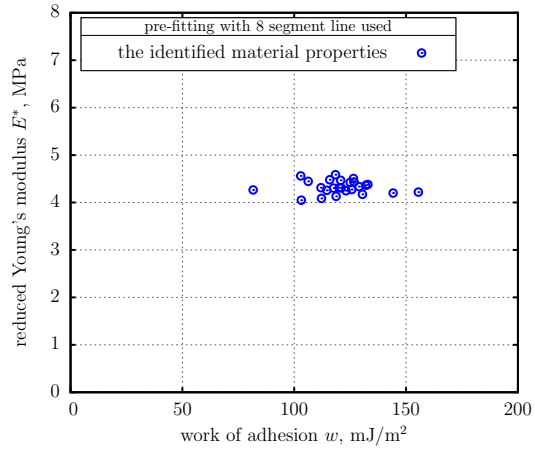


(c)

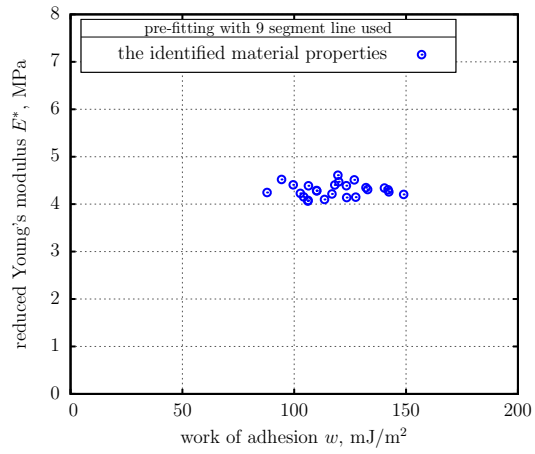
Figure A.19: Material properties extracted using pre-fitting with polygonal chain. Number of segments in chain are correspondingly 4 (a), 5 (b), 6 (c).



(a)



(b)



(c)

Figure A.20: Material properties extracted using pre-fitting with polygonal chain. Number of segments in chain are correspondingly 7 (a), 8 (b), 9 (c).

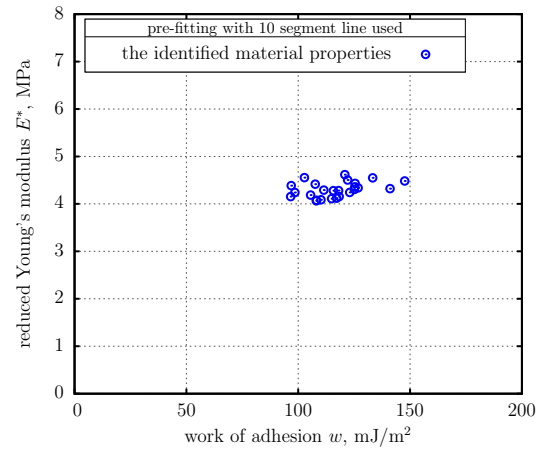


Figure A.21: Material properties extracted using pre-fitting with polygonal chain. Number of segments in chain: 10.